Available online at www.sciencedirect.com

SciVerse ScienceDirect

Ceramics International 39 (2013) 7255–7261

CERAMICS INTERNATIONAL

www.elsevier.com/locate/ceramint

Short communication

One step hydrothermal synthesis of micro-belts like β-$Ni(OH)_2$ thin films for supercapacitors

Girish S. Gund[a], Deepak P. Dubal[b], Sujata S. Shinde[a], Chandrakant D. Lokhande[a,*]

[a]*Thin Film Physics Laboratory, Department of Physics, Shivaji University, Kolhapur 416004, M.S., India*
[b]*Technische Universität Chemnitz, Institut für Chemie, AG Elektrochemie, D-09107 Chemnitz, Germany*

Received 25 December 2012; received in revised form 24 January 2013; accepted 25 January 2013
Available online 1 February 2013

Abstract

Present investigation deals with synthesis of micro-belts-like $Ni(OH)_2$ thin film by the hydrothermal method. $Ni(OH)_2$ thin films are characterized by the X-ray diffraction (XRD), scanning electron microscopy (SEM), Fourier transform infrared spectroscopy (FTIR) and surface wettability techniques. The XRD and FTIR analyses confirm the formation of β-$Ni(OH)_2$ thin films. SEM analysis reveals the development of three dimensional growths of randomly distributed interconnected micro-belts. The electrochemical properties of β-$Ni(OH)_2$ in 2 M KOH electrolyte shows the pseudocapacitive behavior with the specific capacitance of 324 F g^{-1} and capacitive retention of 78% after 500 cycles. The values of specific energy and power are found to be 1.36 Wh kg^{-1} and 50 W kg^{-1}, respectively. Additionally, impedance analysis reveals that micro-belt like $Ni(OH)_2$ provides less electrochemical series resistance.

Keywords: Nickel hydroxide; Micro-belts; Hydrothermal synthesis; Supercapacitor

1. Introduction

Recently, the material scientists have been mostly focused on the synthesis of different nanostructured metal oxides/hydroxides because of their prospectus applications in diverse areas. Furthermore, the metal hydroxides have layered structure, complex forming behavior, multivalent nature, high thermal stability and ease of preparation. In metal hydroxides and oxides brucite-like structured materials have excellent applications in different fields, which mostly depend on structural features [1]. Nickel hydroxide ($Ni(OH)_2$) is one of the super-prospective material having four polymorphs namely: α-$Ni(OH)_2$, β-$Ni(OH)_2$, β-NiOOH and γ-NiOOH [2]. Out of these α and β polymorphs are mostly and easily obtained forms. α-$Ni(OH)_2$ consists of a stacked $Ni(OH)_{2-x}$ layer intercalated with different anions or water molecules and is isostructural with hydrotalcite-like material while anhydrous β-$Ni(OH)_2$ has a brucite-like structure [3]. The α and β polymorphs of $Ni(OH)_2$ have different properties such as chemical structure, degree of hydration and morphology.

Based on the charge storage mechanism, there are two major categories of supercapacitors: (1) electric double-layer capacitors (EDLC) which store energy by utilizing the double-layer capacitance arising from the charge separation at the electrode–electrolyte interface and (2) pseudocapacitors which store energy by utilizing the pseudocapacitance arising from fast and reversible faradic reactions [4]. Recently, the main materials that have been studied for the supercapacitor electrode are (i) carbon polymorphs (ii) transition metal oxides and (iii) conducting polymers. Transition metal oxides/hydroxides have received increasing interest as an alternative to carbons and conducting polymers for supercapacitors as well as for battery applications. Among them, nickel hydroxide is a most promising electrode material for supercapacitors due to its low cost, natural abundance, low toxicity and high theoretical specific capacitance [5].

Prior to this, $Ni(OH)_2$ has been prepared by various chemical methods viz., microwave irradiation [6], solvothermal

*Corresponding author. Tel.: +91 231 2609225; fax: +91 231 269233.
E-mail addresses: grsh.gund@gmail.com (G.S. Gund), dubaldeepak2@gmail.com (D.P. Dubal), sujata.surwase@gmail.com (S.S. Shinde), l_chandrakant@yahoo.com (C.D. Lokhande).

0272-8842/$ - see front matter © 2013 Elsevier Ltd and Techna Group S.r.l. All rights reserved.
http://dx.doi.org/10.1016/j.ceramint.2013.01.091

[5], reflux [7], chemical bath deposition [8], spin coating [9], successive ionic layer adsorption, the reaction method [3] etc. Direct preparation of $Ni(OH)_2$ in thin film form by the hydrothermal method is less investigated. Usually the hydrothermal method results into powdered form and further by using binder and different additives this powder is pressed on the current collector in order to make electrode [9].

In the present work, we have synthesized micro-belts like $Ni(OH)_2$ thin film using the single step hydrothermal method. This avoids the steps like powder dispersion in solvent and use of binders, additives etc. for better adhesion. The hydrothermal method is the most attractive method due to its simplicity, reproducibility and environmental friendly nature etc. It is well suited for large-area deposition at low temperature (<473 K), as it avoids the oxidation/corrosion of metallic substrates. The electrochemical supercapacitive behavior and long-term operation stability of micro-belts like $Ni(OH)_2$ thin films were evaluated using the cyclic voltammetry, galvanostatic charge–discharge and electrochemical impedance spectroscopy.

2. Experimental details

Nickel nitrate ($Ni(NO_3)_2.6H_2O$) and ammonium hydroxide (NH_4OH) (AR grade) were used as precursors. Synthesis of micro-belts like $Ni(OH)_2$ thin film by the hydrothermal method is based on heating in an alkaline bath of 0.1 M $Ni(NO_3)_2$ containing the substrates immersed vertically in the solution under the closed system. Briefly, $Ni(NO_3)_2$ solution was complexed with ammonium hydroxide and pH of the solution was maintained at $\sim$12. The well-cleaned stainless steel/glass substrates were dipped in the prepared solution bath and kept in hydrothermal autoclave. When the temperature of the system was reached to 353 K, the system pressure rose above 1 atm and the precipitation (greenish in color) was started in the bath. During the precipitation, deposition of nickel hydroxide took place on the substrate. The temperature of the system was maintained at 353 K for 12 h. After 12 h, stainless steel substrates coated with $Ni(OH)_2$ thin films were taken out, dried in air and used for further characterizations [10].

The $Ni(OH)_2$ thin films were deposited by using the Equitron autoclave-pad (port/mini). For the structural elucidation of the film, X-ray diffraction analysis was performed using Bruker axs D8 Advance Model with K_α radiations ($\lambda=1.54$ Å). The FTIR spectrum of the sample was collected using a 'PerkinElmer, FTIR Spectrum one' unit. The surface morphology of the film was visualized using scanning electron microscopy (SEM JEOL-JAPAN 6360). The cyclic voltammetry and galvanostatic charge–discharge measurements were performed with Automatic Battery Cycler (WBCS3000). An electrochemical impedance measurement was carried out using the electrochemical workstation (ZIVE SP5).

3. Results and discussion

3.1. Film formation and reaction mechanism

Synthesis of micro-belts like $Ni(OH)_2$ thin film by the hydrothermal method is based on the heating of an alkaline bath of nickel nitrate containing substrates under controlled pressure (>1 atm) and temperature (353 K). The pressure together with temperature advances the arrangement of molecules, since all liquids have assured vapor pressure and it increases with temperature for the closed system. So, better adhesion with improved crystalline structure and morphology of the film can be obtained. In thin film formation, nucleation on the substrate takes place and further growth on nucleation sites creates clusters, this may be due to the hasty decomposition of metal complex molecules. Consequently the film grows to a certain thickness on the substrate surface by the coalescence of particles [11]. For deposition of $Ni(OH)_2$ films, 0.1 M $Ni(NO_3)_2$ was used as a source of nickel. The process of film formation is discussed as follows: Initially, $Ni(NO_3)_2$ salt is dissolved in water so nickel hydrated ions are produced in the bath as shown in Fig. 1(a) and explained with the following reaction [3]:

$$Ni(NO_3)_2\cdot 6H_2O+(n+x)H_2O\rightarrow[Ni(H_2O)_{(x+6)}]^{2+}+2[NO_3(H_2O)_{n/2}]^- \quad (1)$$

Addition of ammonium hydroxide replaces the H_2O ligands by OH^- around the Ni^{2+} species because of its high reactivity and greenish murky $Ni(OH)_2$ precipitation is formed at pH $\approx$ 10 which is shown in Fig. 1(b) and can be explained with the following reaction:

$$m[Ni(H_2O)_{(x+6)}]^{2+}+2m(NH_4OH)\rightarrow m[Ni(OH)_2]\downarrow+2m(NH_4^+)+m(x+6)(H_2O) \quad (2)$$

Further addition of ammonium hydroxide dissolves precipitate and forms $Ni(NH_3)_q^{2+}$ complex ion by replacing OH^- ligands around Ni^{2+}, where $q=1$–4 in which 4 is the most stable coordination number. However, clear blue solution is obtained at pH value close to 12 as shown in Fig. 1(c) and explained with the following reaction:

$$m[Ni(OH)_2]+q(NH_4^+)+q(OH^-)\rightarrow m[Ni(NH_3)_q^{2+}]+q(H_2O)+q(OH^-) \quad (3)$$

The stainless steel/glass substrates were dipped vertically in the solution kept in an autoclave and temperature is maintained at 353 K for 12 h. When bath attains the temperature of 353 K, NH_3 molecules are liberated from the solution. The release of NH_3 molecules disturbs the stability and pH of the solution. Thus, the decomposition of $Ni(NH_3)q^{2+}$ complex takes place by releasing NH_3 gas as shown in Fig. 1(d) and described with the following equation:

$$m[Ni(NH_3)_q^{2+}]+2m(OH^-)\rightarrow m[Ni(OH)_2]+q(NH)_3\uparrow \quad (4)$$

When this solution along with the immersed substrates is heated to 353 K, the solution once again becomes saturated;

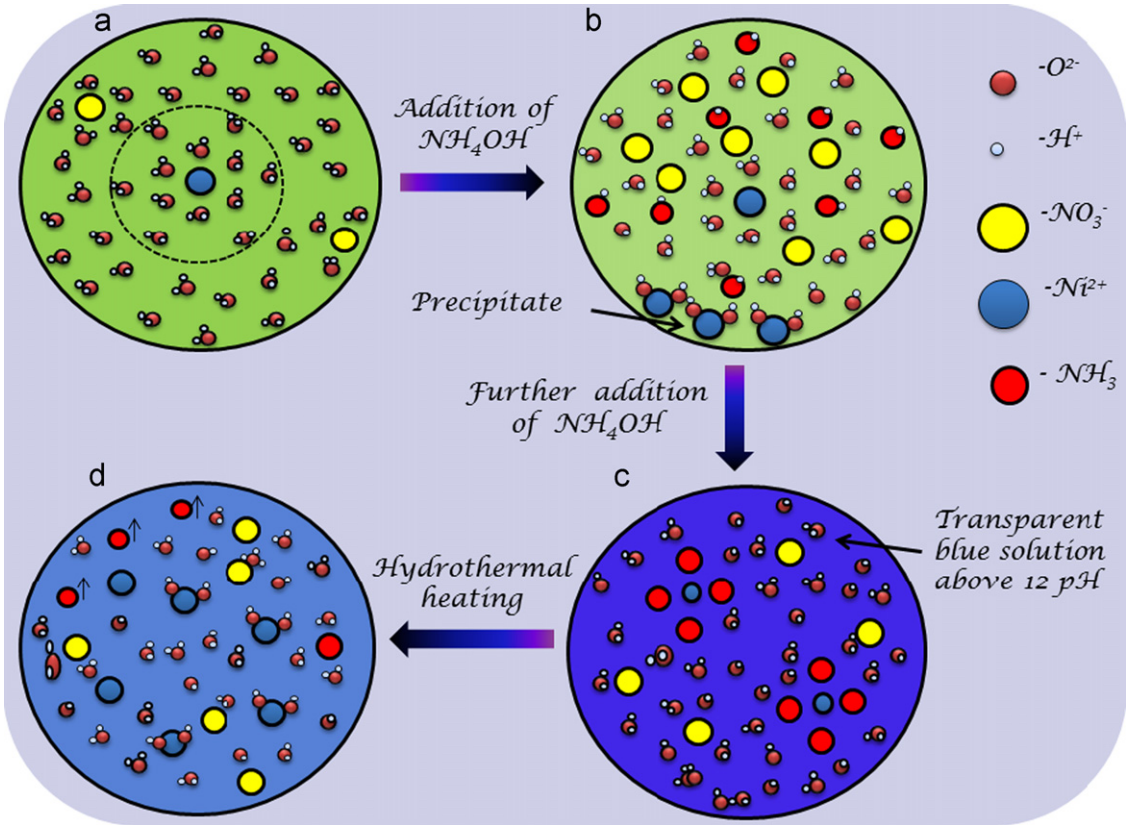

Fig. 1. Schematic representation for the reactions in solution bath: (a) Dissolution of $(NO_3)_2.6H_2O$ in double distilled water. (b) Addition of ammonium hydroxide upto 10 pH causes greenish precipitate in bath. (c) Further addition of ammonium hydroxide dissolves precipitate (at ~12pH) and results into clear solution. (d) Formation of $Ni(OH)_2$ and release of NH_3 from the solution due to the hydrothermal heating at 353K. (For interpretation of the references to color in this figure legend, the reader is referred to the web version of this article.)

the ionic product exceeds the solubility product and precipitation occurs via heterogeneous growth on the substrate. When the ionic product starts to exceed the solubility product, nickel hydroxide nuclei are produced both on the substrate and in the solution. Thus, they serve as ideal building blocks and tend to assemble into nanostructures. This is the start of the nucleation of the $Ni(OH)_2$ material, and consequently these nuclei grow into micro-belts on the substrates. In the next stage of the reaction, as the ionic product progressively increases, nanoparticles are collected on these micro-belts and collectively grow to form thick micro-belts.

3.2. X-ray diffraction

Fig. 2(a) shows the XRD pattern of $Ni(OH)_2$ thin film deposited on the glass substrate. The XRD pattern shows the polycrystalline nature of $Ni(OH)_2$ thin films having brucite-like hexagonal crystal phase (JCPDS file no. 01-1047) [12]. The crystallite size of β-$Ni(OH)_2$ was calculated on the basis of full width at half maxima intensity of most intense XRD peak by using Scherrer's formula,

$$D = \frac{0.9\lambda}{\beta \cos\theta} \quad (5)$$

where 'D' is the average crystallite size, 'β' is the full width at half maxima, 'λ' is the wavelength of X-ray used and 'θ' is the diffraction angle. The β-$Ni(OH)_2$ has a particle size ~52 nm for the (001) plane. The crystallite size of 29 nm was reported by Patil et al. for β-$Ni(OH)_2$ thin film deposited by the chemical bath deposition method [8] and Kulkarni et al. estimated 41 nm crystallite size for SILAR deposited thin film of β-$Ni(OH)_2$ [3]. In the present case, β-$Ni(OH)_2$ is more crystalline due to suitability of the hydrothermal method for improving crystallinity, which is in consistent with the literature [13–15].

3.3. FT-IR spectroscopy

Fig. 2(b) shows the FTIR spectrum that reveals the chemical information and major functional groups present in the β-$Ni(OH)_2$. The sharp peak at 3641 cm^{-1} and a wide band at 3445 cm^{-1} are headed for the non-hydrogen bounded hydroxyl groups (γOH), symmetric stretching vibrational mode and hydrogen bounded hydroxyl groups stretching vibrational mode in the β-$Ni(OH)_2$, respectively [12]. The peaks at 459 and 545 cm^{-1} are credited to the Ni–OH stretching vibration for β-$Ni(OH)_2$ [3,12]. Since metal hydroxides are basic in nature, there is adsorption of atmospheric

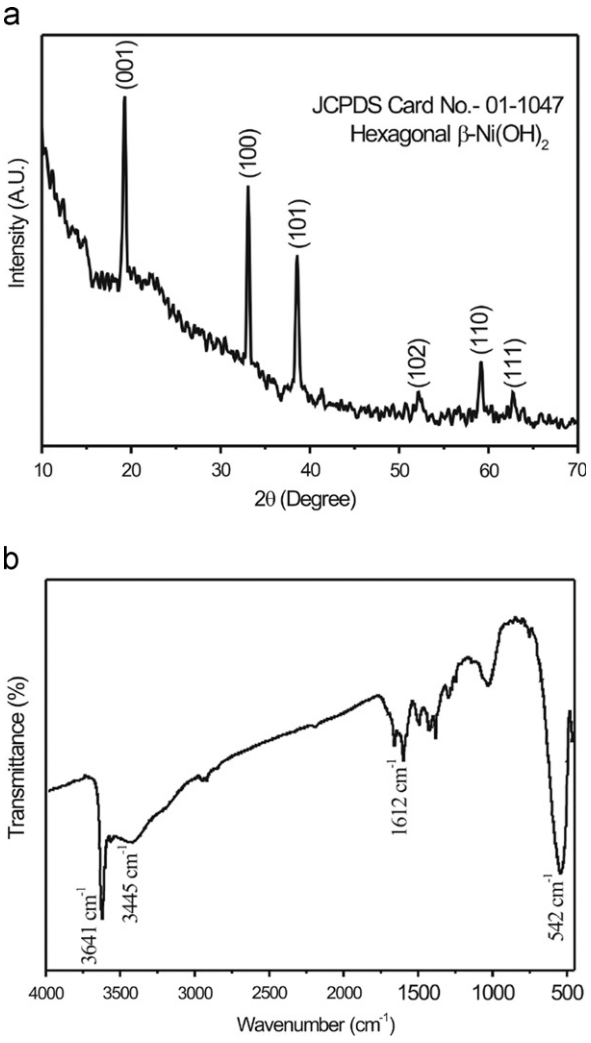

Fig. 2. (a) X-ray diffraction pattern of β-Ni(OH)$_2$ thin film on glass substrate. (b) FTIR spectrum of Ni(OH)$_2$ sample.

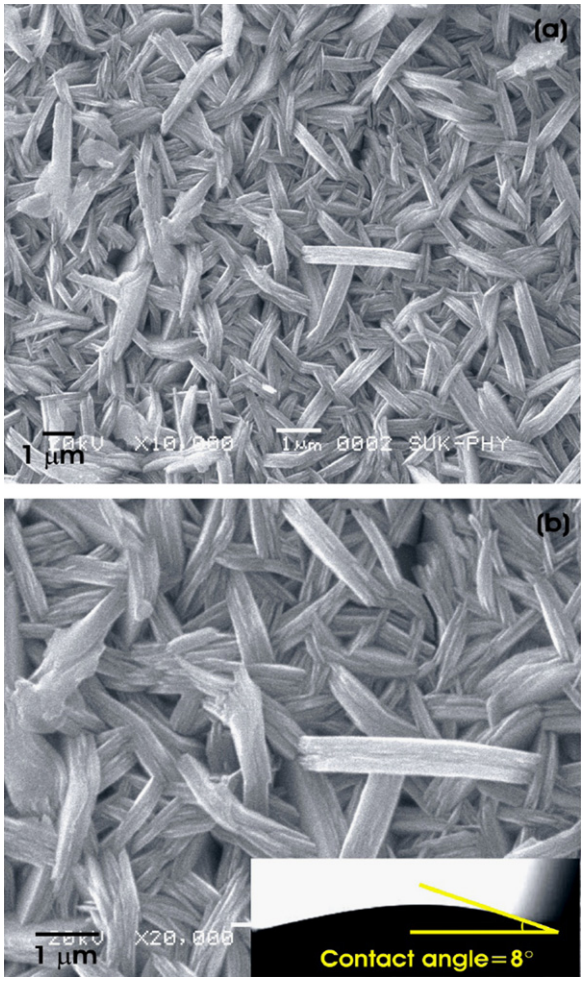

Fig. 3. (a),(b) Scanning electron micrographs of β-Ni(OH)$_2$ thin film at two different magnifications. Inset of (b) shows photograph of water droplet on Ni(OH)$_2$ film surface with contact angle 8°.

carbon dioxide on it and occurrence of carbonate anions on β-Ni(OH)$_2$ surface is confirmed by minor peak at 1441 cm^{-1} [12]. The small absorption peaks at 1027, 1301, 1380, 1612 and 1660 cm^{-1} are ascribed to the vibrational mode of surface adsorbed nitrate ions (NO_3^-) which are from the preliminary nickel nitrate solution [12,16]. These characteristic bonds confirm the formation of Ni(OH)$_2$ thin films.

3.4. Scanning electron microscopy

Fig. 3(a) and (b) shows the SEM images of Ni(OH)$_2$ thin films deposited at two different magnifications. At low magnification, it is seen that Ni(OH)$_2$ film surface is well covered with smooth, irregular shaped micro-belts of random size. While at high magnification, we found the voids and pores between interconnected micro-belts and approximate length of the micro-belts is about 1–2 μm in range. Using the hydrothermal method, different types of surface morphologies of Ni(OH)$_2$ have been reported [17]. Nano-particles have been synthesized by Jayalakshmi et al. using hydrous nickel nitrate and urea bath at 403 K temperature [18], Zhuo et al. obtained nanotubes by utilizing solution of nickel nitrate, ammonia solution and $NaNO_3$ at 523 K [19]. Platelet-like nanoparticles have been synthesized by Meyer et al. using solution bath of nickel nitrate with different alkaline media (ammonia, methylamine, trimethylammonium and potassium hydroxide) at 373 K [20]. In this work, the obtained micro-belts like morphology implies good surface area with porous structure, which is beneficial for accessing the active material to electrolyte ions and offers easy path for migration of ions and faradic reaction.

Wettability is the ability of liquid to spread on the solid material which can be calculated by determining contact angle measurement. The wetting behavior of solid with water is dependent on the properties of solid surface (like surface energy, surface roughness etc.) and liquid used [21]. Wettability study is an important technique to examine the interaction between aqueous electrolyte and nickel hydroxide electrode. In the present case, water lies with contact angle of 8° on the surface of β-Ni(OH)$_2$ thin film forming a

droplet as seen in the inset of Fig. 3(b), indicating super-hydrophilic behavior which is helpful for good ion exchange at interface [22]. This is useful for making the intimate contact of aqueous electrolyte with $Ni(OH)_2$ thin film electrode. The SEM images reveal the presence of voids and pores between interconnected micro-belts. So water placed on the surface of film goes inside the voids and pores around the micro-belts. Superhydrophilicity is ascribed to the nanocrystalline nature of material and both these properties are the prime requirements for good supercapacitor electrode material [23].

3.5. Electrochemical supercapacitive study

3.5.1. Cyclic voltammetry

The cyclic voltammetry (CV) technique was employed to evaluate the supercapacitive properties of β-$Ni(OH)_2$ electrode on stainless steel substrate. Fig. 4(a) displays a typical CV curves of β-$Ni(OH)_2$ electrode in 2 M KOH electrolyte at different scan rates in the potential range 0–+0.45 V/SCE. The shape of the CV curves indicate that the capacitive characteristics are mainly raised due to the pseudo-capacitance based on the redox mechanism, and not from electric double layer which has nearly rectangular shape. The appearance of anodic and cathodic peaks corresponds to the β-$Ni(OH)_2$/β-NiOOH redox reaction in the CV according to the following electrochemical reaction:

$$\beta\text{-}Ni(OH)_2 + OH^- \leftrightarrow \beta\text{-}NiOOH + H_2O + e^-$$
$$\text{charging} \leftrightarrow \text{discharging} \quad (6)$$

The capacitance (C) was calculated using the following relation:

$$C = \frac{I_{max}}{dV/dt} \quad (7)$$

The specific capacitance Cs (Fg^{-1}) of $Ni(OH)_2$ electrode was evaluated using the following relation:

$$Cs = \frac{C}{W} \quad (8)$$

where W is the deposited weight of $Ni(OH)_2$ on thin film for unit area (1 cm^2) dipped in the electrolyte. In the present study, specific capacitance for the micro-belt structured β-$Ni(OH)_2$ thin film electrode is found to be 324 F g^{-1} at 5 m V s^{-1} scan rate.

The $Ni(OH)_2$ material is attractive because of its well-defined electrochemical redox activity and the possibility of improved performance through different preparative methods [24]. Patil et al. synthesized β-$Ni(OH)_2$ thin films by CBD and reported the specific capacitance of 398 F g^{-1} [8]. Kulkarni et al. obtained specific capacitance of 350 F g^{-1} for SILAR deposited $Ni(OH)_2$ thin films [3]. Inset of Fig. 4 shows the variation of specific capacitance with scan rate. The specific capacitance values decreased from 324 to 32 F g^{-1} as the scan rate increases from 5 to 100 m V s^{-1}. The intercalation of OH^- ions from the solution to the surface of active material of electrode takes adequate time for charging and discharging. The OH^- ions take longer time for intercalation/deintercalation at slow scan rate and transfer more charges compare to higher scan rate, which results into a higher specific capacitance at slow scan rate [25].

3.5.2. Stability study

The long-term operation stability of the micro-belts like β-NiOH electrode was investigated by the CV cycling as shown in Fig. 5. There is slight increment in the capacity retention up to 100 cycles then it starts to decrease. The enhancement in capacitance and capacity retention up to 100 cycles may be attributed to the integration of voltammetric charges for the positive and negative sweeps of the CVs [26]. Further, cycling results into decrement in the specific capacitance, which may be due to the dissolution

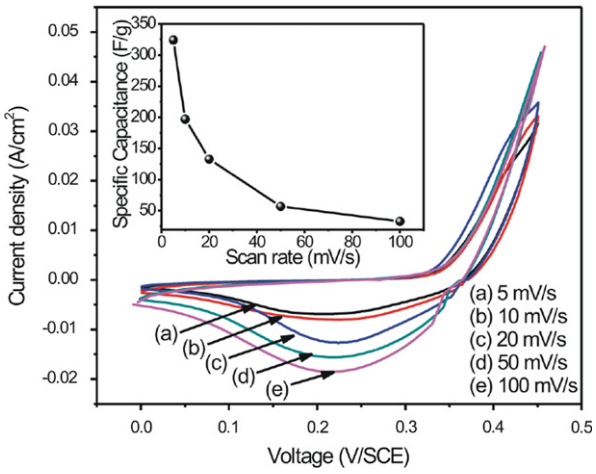

Fig. 4. Cyclic voltammograms curves of micro-belts like $Ni(OH)_2$ electrode at different scanning rates. Inset shows variation of specific capacitance with scan rates in 2 M KOH electrolyte.

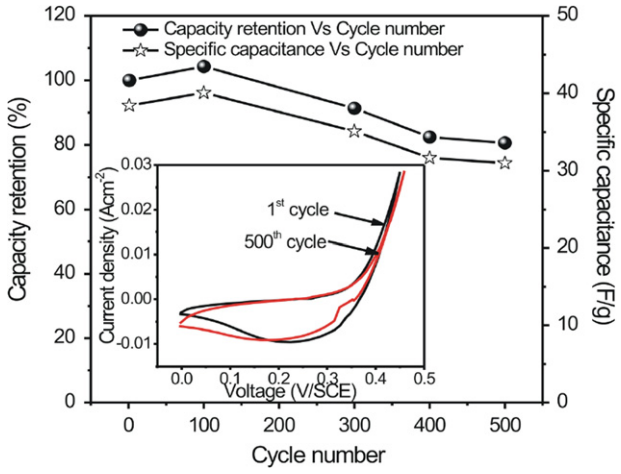

Fig. 5. Plots of variation of specific capacitance and capacity retention with respect to cycle numbers. Inset shows the CV curves of $Ni(OH)_2$ electrode at different cycles at 100 m V s^{-1} scan rate.

and/or detachment of active material during the early charging/discharging cycles in the electrolyte [27]. The capacity retention of 78% is obtained after 500 cycles at 100 m V s^{-1} scan rate.

3.5.3. Galvanostatic charge–discharge study

Fig. 6(a) shows the charge–discharge curve of the $Ni(OH)_2$ thin film in 2 M KOH electrolyte at current density of 0.1 mA cm^{-2}. The charge–discharge curve is asymmetric in nature and reflects the pseudocapative behavior of $Ni(OH)_2$ thin film. In addition, there is an initial drop in potential, which may be due to the internal resistance of $Ni(OH)_2$ electrode. The specific energy (S.E.) and specific power (S.P.) were calculated from the discharge curves:

$$\text{S.E.} = \frac{VI_dT_d}{W} \tag{9}$$

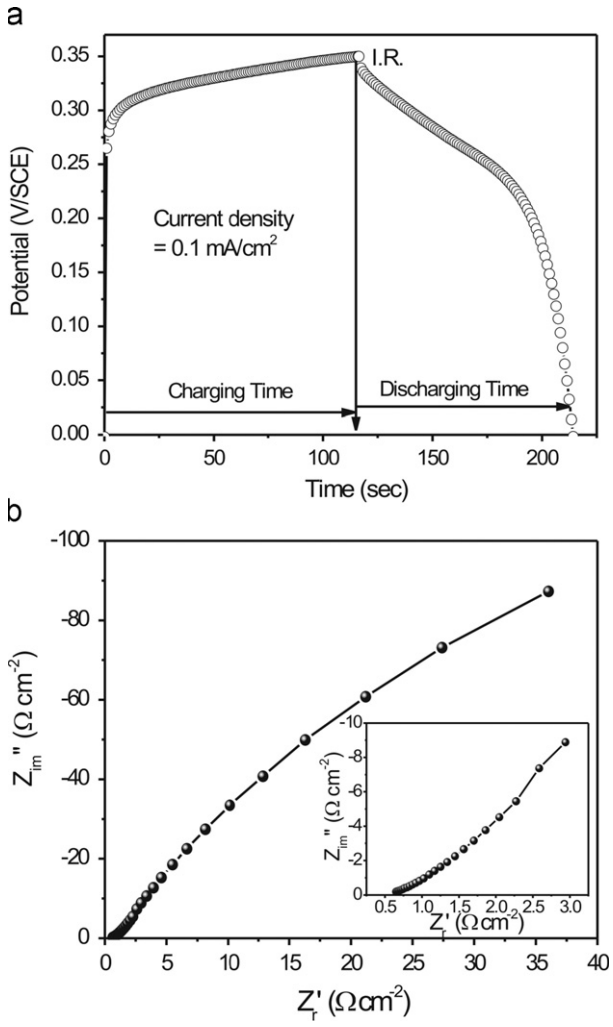

Fig. 6. (a) Galvanostatic charge–discharge curve of β-$Ni(OH)_2$ micro-belts at current density 0.1 mA cm^{-2}. (b) Nyquist plot of β-$Ni(OH)_2$ micro-belts at 0.1 V/SCE from 10^5 to 10^{-1} Hz frequency range and the inset shows enlarged view of the Nyquist plot in the high frequency region.

$$\text{S.P.} = \frac{VI_d}{W} \tag{10}$$

where I_d is the constant discharge current, T_d is the discharge time, W is the active mass and V is the potential drop during discharge. The values of specific energy and specific power are found to be 1.36 Wh kg^{-1} and 50 W kg^{-1}, respectively. The highest specific energy of 77.8 Wh kg^{-1} was obtained by Yan et al. for the asymmetric supercapacitors based on $Ni(OH)_2$/graphene and porous graphene [28]. Lang et al. reported the maximum specific power of 1.1 kW kg^{-1} for asymmetric supercapacitors based on stabilized α-$Ni(OH)_2$ and activated carbon [29].

3.5.4. Electrochemical impedance spectroscopy

The electrochemical impedance spectroscopy (EIS) was evaluated to measure the mechanistic aspects of $Ni(OH)_2$ electrode at +0.1 V/SCE and in the 10^5–10^{-1} Hz frequency range. Fig. 6(b) shows the Nyquist plot of the $Ni(OH)_2$ electrode in the steady state. The equivalent series resistance of a supercapacitor consists of electronic and ionic contributions [30,31]. The electronic resistance is related to intrinsic resistance of the material whereas interfacial resistance corresponds to inter-particles resistance and resistance between particles and current collector. The ionic resistance is associated with the electrolyte resistances in the pores and the ionic (diffusion) resistance of ions moving in small pores. The equivalent series resistance (ESR) of electrode can be obtained from the intercept of real impedance at high frequencies. The ESR of $Ni(OH)_2$ electrode is found to be 0.65 Ω, which entails the lower electronic and ionic resistance. The steeper nature of the slope in the lower frequency region demonstrates the better capacitive performance. Lang et al. reported 1.58 Ω of ESR for loose-packed $Ni(OH)_2$ nanoflakes [32]. This implies that the electrochemical reaction on micro-belts structured electrode proceeds more easily.

4. Conclusions

In conclusion, we have synthesized micro-belts like β-$Ni(OH)_2$ thin films with hexagonal structure by the single step hydrothermal method. The micro-belt structured $Ni(OH)_2$ electrode demonstrated excellent supercapacitive behavior with the specific capacitance of 324 F g^{-1} at a scan rate of 5 m V s^{-1} and capacity retention of 78% after 500 cycles. Also, the galvanostatic charge–discharge study disclosed the effective electrochemical performance of microbelts-like $Ni(OH)_2$ thin films. The EIS measurement shows that micro-belts like β-$Ni(OH)_2$ electrode offer very low impedance and causes easy access to ions for intercalation and de-intercalation. Thus, micro-belts like β-$Ni(OH)_2$ electrode are promising materials for supercapacitor application.

Acknowledgment

Authors are grateful to the Council for Scientific and Industrial Research (CSIR), New Delhi (India) for financial support through Scheme no. 03(1165)/10/EMR-II. Authors are also grateful to Department of Science and Technology for financial support through PURSE and FIST & University Grant Commission (UGC) through DSA-I scheme.

References

[1] C.D. Lokhande, D.P. Dubal, O.S. Joo, Metal oxide thin film based supercapacitors, Current Applied Physics 11 (2011) 255.
[2] X. Kong, X. Liu, Y. He, D. Zhang, X. Wang, Y. Li, Hydrothermal synthesis of β-nickel hydroxide microspheres with flake like nanostructures and their electrochemical properties, Materials Chemistry and Physics 106 (2007) 375.
[3] S.B. Kulkarni, V.S. Jamdade, D.S. Dhawale, C.D. Lokhande, Synthesis and characterization of β-$Ni(OH)_2$ up grown nanoflakes by SILAR method, Applied Surface Science 255 (2009) 8390.
[4] D.P. Dubal, S.H. Lee, J.G. Kim, W.B. Kim, C.D. Lokhande, Porous polypyrrole clusters prepared by electropolymerization for a high performance supercapacitor, Journal of Materials Chemistry 22 (2012) 3044.
[5] X. Zhang, W. Shi, J. Zhu, W. Zhao, J. Zhao, J. Ma, S. Mhaisalkar, J.L. Maria, Y. Yang, H. Zhang, H.H. Hng, Q. Yan, Synthesis of porous NiO nanocrystals with controllable surface area and their application as supercapacitor electrodes, Nano Research 3 (2010) 643.
[6] S.K. Meher, P. Justin, G.R. Rao, Microwave-mediated synthesis for improved morphology and pseudocapacitance performance of nickel oxide, Applied Materials and Interfaces 3 (2011) 2063.
[7] J.W. Lee, T. Ahn, J.H. Kim, J.M. Ko, J.D. Kim, Nanosheets based mesoporous NiO microspherical structures via facile and template-free method for high performance supercapacitors, Electrochimica Acta 56 (2011) 4849.
[8] U.M. Patil, K.V. Gurav, V.J. Fulari, C.D. Lokhande, O.S. Joo, Characterization of honeycomb-like β-$Ni(OH)_2$ thin films synthesized by chemical bath deposition method and their supercapacitor application, Journal of Power Sources 188 (2009) 338.
[9] A.A. Al-Ghamdi, W.E. Mahmoud, S.J. Yaghmour, F.M. Al-Marzouki, Structure and optical properties of nanocrystalline NiO thin film synthesized by sol–gel spin-coating method, Journal of Alloys and Compounds 486 (2009) 9.
[10] D.P. Dubal, A.D. Jagadale, C.D. Lokhande, Big as well as light weight portable, Mn_3O_4 based symmetric supercapacitive devices: fabrication, performance evaluation and demonstration, Electrochimica Acta 80 (2012) 160.
[11] R.S. Mane, C.D. Lokhande, The chemical deposition method for metal chalcogenide thin films, Materials Chemistry and Physics 65 (2000) 1.
[12] S.M. Zhang, H.C. Zeng, Self-assembled hollow spheres of β-$Ni(OH)_2$ and their derived nanomaterials, Chemicals Materials 21 (2009) 871.
[13] C. Li, S. Liu, Preparation and characterization of $Ni(OH)_2$ and NiO mesoporous nanosheets, Journal of Nanomaterials 2012 (2012) 648012, 6.
[14] M.H. Cao, T.F. Liu, S. Gao, Single-crystal dendritic micro-pines of magnetic α-Fe_2O_3: large-scale synthesis, formation mechanism, and properties, Angewandte Chemie International Edition 44 (2005) 4197.
[15] H.B. Liu, L. Xiang, Y. Jin, Hydrothermal modification and characterization of $Ni(OH)_2$ with high discharge capability, Crystal Growth and Design 6 (2006) 283.
[16] F. Prinetto, G. Ghiotti, I. Nova, L. Lietti, E. Tronconi, P. Forzatti, In situ FTIR and reactivity study of NO_x storage over Pt–Ba/Al_2O_3 catalysts, Journal of Physical Chemistry B 105 (2011) 12732.
[17] D.P. Dubal, V.J. Fulari, C.D. Lokhande, Effect of morphology on supercapacitive properties of chemically grown β-$Ni(OH)_2$ thin films, Microporous and Mesoporous Materials 151 (2012) 511.
[18] M. Jayalakshmi, M.M. Rao, K. Kim, Effect of particle size on the electrochemical capacitance of α-$Ni(OH)_2$ in alkali solutions, International Journal of Electrochemical Science 1 (2006) 324.
[19] L. Zhuo, J. Ge, L. Cao, B. Tang, Solvothermal synthesis of CoO, Co_3O_4, $Ni(OH)_2$ and $Mg(OH)_2$ nanotubes, Crystal Growth and Design 9 (2009) 1.
[20] M. Meyer, A. Bee, D. Talbot, V. Cabuil, J.M. Boyer, B. Repetti, R. Garrigos, Synthesis and dispersion of $Ni(OH)_2$ platelet-like nanoparticles in water, Journal of Colloid and Interface Science 277 (2004) 309.
[21] R. Pogreb, G. Whyman, R. Barayev, E. Bormashenko, D. Aurbach, A reliable method of manufacturing metallic hierarchical superhydrophobic surfaces, Applied Physics Letters 94 (2009) 221902.
[22] O. Bockman, T. Ostvold, G.A. Voyiatzis, G.N. Papatheodorou, Raman spectroscopy of cemented cobalt on zinc substrates, Hydrometallurgy 55 (2000) 93.
[23] P.M. Kulal, D.P. Dubal, C.D. Lokhande, V.J. Fulari, Chemical synthesis of Fe_2O_3 thin films for supercapacitor application, Journal of Alloys and Compounds 509 (2011) 2567.
[24] G. Yang, C. Xu, H. Li, Electrodeposited nickel hydroxide on nickel foam with ultrahigh capacitance, Chemical Communications 48 (2008) 6537.
[25] D.P. Dubal, S.V. Patil, A.D. Jagadale, C.D. Lokhande, Two step novel chemical synthesis of polypyrrole nanoplates for supercapacitor application, Journal of Alloys and Compounds 509 (2011) 8183.
[26] D.P. Dubal, D.S. Dhawale, R.R. Salunkhe, C.D. Lokhande, Conversion of chemically prepared interlocked cube-like Mn_3O_4 to birnessite MnO_2 using electrochemical cycling, Journal of Electrochemical Society 157 (2010) A812.
[27] D.P. Dubal, S.V. Patil, W.B. Kim, C.D. Lokhande, Supercapacitors based on electrochemically deposited polypyrrole nanobricks, Materials Letters 65 (2011) 2628.
[28] J. Yan, Z. Fan, W. Sun, G. Ning, T. Wei, Q. Zhang, R. Zhang, L. Zhi, F. Wei, Advanced asymmetric supercapacitors based on $Ni(OH)_2$/graphene and porous graphene electrodes with high energy density, Advanced Functional Materials 22 (2012) 2632.
[29] J. Lang, L. Kong, M. Liu, Y. Luo, L. Kang, Asymmetric supercapacitors based on stabilized α-$Ni(OH)_2$ and activated carbon, Journal of Solid State Electrochemistry 14 (2010) 1533.
[30] D.P. Dubal, D.S. Dhawale, T.P. Gujar, C.D. Lokhande, Effect of different modes of electrodeposition on supercapacitive properties of MnO_2 thin films, Applied Surface Science 257 (2011) 3378.
[31] A.G. Pandolfo, A.F. Hollenkamp, Carbon properties and their role in supercapacitors, Journal of Power Sources 157 (2006) 11.
[32] J. Lang, L. Kong, W. Wu, M. Liu, Y. Luo, L. Kang, A facile approach to the preparation of loose-packed $Ni(OH)_2$ nanoflake materials for electrochemical capacitors, Journal of Solid State Electrochemistry 13 (2009) 333.